Proceedings Paper:
Da, C, Hudson, S orcid.org/0000-0003-3919-5266, Richardson, R et al. (1 more author) (2020) An Upper Limb Fall Impediment Strategy for Humanoid Robots. In: Lecture Notes in Computer Science. TAROS 2020: 21st Towards Autonomous Robotic Systems Conference, 16 Sep 2020, Nottingham, UK. Springer Nature . ISBN 978-3-030-63485-8

https://doi.org/10.1007/978-3-030-63486-5_34

An Upper Limb Fall Impediment Strategy for Humanoid Robots

Da Cui[1,2], Samuel Hudson[1], Robert Richardson[1], and Chengxu Zhou[1]

[1] School of Mechanical Engineering, University of Leeds, UK.
[2] School of Mechanical and Aerospace engineering, Jilin University, China.
C.X.Zhou@leeds.ac.uk

Abstract. Falling is an unavoidable problem for humanoid robots due to the inherent instability of bipedal locomotion. In this paper, we present a novel strategy for humanoid fall prevention by using environmental contacts. Humans favour to contact using the upper limbs with the proximate environmental object to prevent falling and subliminally or consciously select a pose that can generate suitable Cartesian stiffness of the arm end-effector. Inspired by this intuitive human interaction, we design a configuration optimization method to choose a well thought pose of the arm as it approaches the long axis of the stiffness ellipsoid, with the displacement direction of the end-effector to utilize the joint torques. In order to validate the proposed strategy, we perform several simulations in MATLAB & Simulink, in which this strategy proves to be effective and feasible.

1 Introduction

Due to the inherent instability of bipedal locomotion and the complexity of work scenarios [17], falling is a common risk for humanoid robots. This shortcoming is one of the key limitations that restrict the application in more general workspaces of these robots. To overcome this problem, there has been various balance control methods proposed, which can be categorized into: ankle [14], hip [23], stepping [15, 19], heuristic [5] and online learning [21] strategies. However, if the external force exceeds the maximum capability or an obstacle constrains the stepping space, there is still a risk of falling. Therefore, there has been some advances in the field by proposing such strategies like falling trajectory optimization [18, 22], pose reshaping [17] and adaptive compliance control [16]. However, these strategies mentioned do not consider wall exploitation or the use of utilizing differentiating environments to avoid falling. In [20], the authors presented a method for exploiting external objects to stabilize a falling robot. This approach uses a simplified three-link model consisting of a contact arm, torso and a stance leg. Besides humanoids, humans also risk falling despite the possession of excellent balance. Subsequently, it is observed that the upper limbs are frequently used to break falls. Based on this observation, Hoffman *et al.* [9] presented a novel strategy using the arms to prevent falling, this strategy combines the passive stiffness of a compliance joint and active stiffness control to obtain a target stiffness of the arm when in contact with the wall.

Research on successful and safe fall arrest strategies of humans has attracted a lot of attention [2,6,7,10,11,13]. Inspired by human reaction and the previous studies mentioned, this paper presents an optimal fall prevention strategy by using upper limbs of humanoid robots. Falls are inevitable for humans, where the upper limbs is frequently used to break falls and primary used to absorb impact [10, 11]. The muscle mechanism is essentially a force dampening system which adjusts the amount of shock accordingly through eccentric contractions about the joints [13]. The joint resistance produced by muscle corresponding deformation is defined as joint stiffness [12]. The pose of arm and joint stiffness play an important role at impact. For example, if the elbow join maintains a high stiffness when contact occurs, it may result in a high damage risk due to under attenuation [2, 3, 7]. On the other hand, low joint stiffness may result in excessive joint gyration, thus not being able to support the body [8]. If the joint has insufficient stiffness due to muscle weakness, the individual can stretch the arm to compensate for this due to there being higher joint stiffness demands to control a forward fall with increased bending of the arm [6, 7].

There is a fine balance between insufficient and excessive joint stiffness that may result in collapse or increase the risk injury respectively [4]. In order to obtain a balanced relationship between joint stiffness, arm pose and arm stiffness, we consider a tool known as the Stiffness ellipsoid which describes specifications of desired force/displacement behavior [1]. The stiffness ellipsoid maps the joint stiffness to end-effector stiffness, whose geometry of the stiffness ellipsoid is affected by the joint stiffness and position. Along the positive long axis of the stiffness ellipsoid, the stiffness of the end-effector can alter over a wide range, completed by the active stiffness control within the joint. Therefore, in order to generate the arm configuration to ensure proper interactions and contact stability for a diverse range of tasks, we set the object to choose an arm pose with the maximum value of the stiffness ellipsoid along the displacement direction of the arm end-effector during contact. This object has two implicit purposes, one is to minimize the angle between the displacement direction and the long axis of the stiffness ellipsoid, and the other one is to maximize the long axis length of the stiffness ellipsoid of the arm end-effector.

The presentation of this work is arranged as follows. Section 2 presents the problems that our strategy addresses. Section 3 details the contact pose optimization algorithm. Section 4 demonstrates simulation results and finally, Section 5 concludes the paper.

2 Problem statement

Consider the scenario demonstrated in Fig. 1, an external force is applied on the robot in the sagittal direction to then push it positively forward. The robot may not be able to maintain balance alone, but can prevent falling by exploiting an external physical object in front of it, where it is defined as a vertical wall in this paper. We assume that the distance between the robot and the wall is known, and the robot must react quickly and efficiently to support itself using only

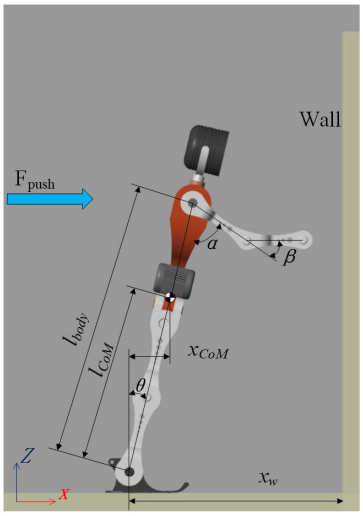

Fig. 1. An illustration of the how the robots fall prevention strategy will operate using the wall

the upper limbs. To solve this problem, we divide the process into three stages: i) fall detection, ii) pre-impact and iii) post-impact. The first step required to prevent the fall, is to detect the fall. The robot needs to judge whether it will fall down based on the information from the sensor. The second pre-impact step, is defined by the time period from when the fall is detected, until impact [8], where it is critical for a pose to be chosen prior to contact with the landing environment. This is where the significance and contributions of this study lie. The post-impact step then describes the movement occurring immediately after impact until stabilization. In this phase, the accumulated momentum during the fall should be absorbed before exceeding the joint limits.

3 Fall prevention strategy

3.1 Fall Detection

A simple method is used for fall detection in this work. When the robot is falling forward due to an external force, the horizontal velocity $\dot{x}_{CoM}$ of the center of mass (CoM) is measured by the onboard inertial measurement unit (IMU). When the measured value exceeds the threshold value $\dot{x}_{th}$ (here $\dot{x}_{th}$ is selected by experience), the arm manoeuvre will be executed in order to prevent falling. Thus, when

$$\dot{x}_{CoM} \geq \dot{x}_{th},$$

the manoeuvre is executed.

3.2 Contact pose optimization

Subsequent to the triggering of the fall prevention manoeuvre, the reaction controller must choose a proper configuration of the arm coming into contact. Our configuration optimizer improves the performance of the arm by using a limited supply of time and actuation power to absorb the momentum accumulated during falling. Due to limited actuation and safety constraints, the undesired momentum cannot be absorbed immediately. However, the momentum must be absorbed before reaching the positional limit (joint limits and environment collision). Therefore, the arm should have necessary compliance to sustain all external forces without body collapse.

For this approach we want to choose a pose of the upper limp that approaches the long axis of the Cartesian stiffness ellipsoid with the direction of the displacement following that of the end-effector. The Cartesian stiffness ellipsoid is described by the following. Consider the upper extremity as an n degrees of freedom manipulator, and whose hand acts as the end-effector, fixed to a wrist in an m-dimensional task space. Let τ, be the joint torque matrix, $\mathbf{q} = [\alpha, \beta]^T$ be the joint configuration containing the shoulder joint, α, and the elbow joint, β, and $\mathbf{K}_q = diag(k_{q_1}, k_{q_2}, k_{q_2}, ..., k_{q_n})$ be the joint stiffness matrix. Assuming there are rigid connections between joints, the relationship between the joint deformation and joint torque, $\delta\mathbf{q}$, can be described as

$$\tau = \mathbf{K}_q \delta\mathbf{q}. \tag{1}$$

Mapping of the joint deformation into Cartesian end-effector displacement $\delta\mathbf{x}$ is described by the linear relation,

$$\delta\mathbf{x} = \mathbf{J}\delta\mathbf{q}, \tag{2}$$

where $\mathbf{J}$ is the forward kinematic Jacobian matrix, where $\mathbf{J} \in \mathbb{R}^{m\times n}$. Consider the relationship between the joint torque τ and the generalized force $\mathbf{F}$ of the end-effector to be

$$\tau = \mathbf{J}^T\mathbf{F}, \tag{3}$$

means we can obtain the extrapolated form

$$\delta\mathbf{x} = \mathbf{J}\mathbf{K}^{-1}\mathbf{J}^T\mathbf{F}. \tag{4}$$

Let, $\mathbf{C} = \mathbf{J}(\mathbf{K}_q)^{-1}\mathbf{J}^T$, be the Cartesian compliance matrix. Where the inverse of $\mathbf{C}$ is $\mathbf{S} = \mathbf{J}^{-1}\mathbf{K}_q(\mathbf{J}^T)^{-1}$ and is the Cartesian stiffness matrix. When one unit deformation occurs at the end-effector,

$$(\delta\mathbf{x})^T(\delta\mathbf{x}) = 1. \tag{5}$$

Now, substituting (4) into (5), obtains

$$\mathbf{F}^T\mathbf{C}^T\mathbf{C}\mathbf{F} = 1. \tag{6}$$

In a given configuration, (6) can represent a m-dimensional force ellipsoid, which is the Cartesian stiffness ellipsoid of the manipulator. A point on the

ellipsoid indicates the magnitude of the generalized force applied on the end-effector, that produces one unit displacement along the direction of that point. The eigenvectors of the matrix constitute of the principal axis of the ellipsoid, and the corresponding eigenvalues, are the inverse square of the semi-axis length of the respective principal axis.

To reach an efficient balance between a soft landing and adequate support, consider the following optimization function:

$$\max_{\mathbf{q}_e} \left\| \mathbf{n}^T \mathbf{S}(\mathbf{q}) \mathbf{n} \right\|, \tag{7}$$

where $\mathbf{q}_e = [\theta, \alpha, \beta]^T$, is the joint position containing the angles of the ankle, shoulder and elbow respectively. $\mathbf{S}(\mathbf{q})$ is the Cartesian stiffness matrix of the arm, $\mathbf{n}$ is the inverse direction vector of the shoulder when contact occurs. In order to avoid calculation of the inverse Jacobian, (7) is changed to minimize the compliance, so that

$$\min_{\mathbf{q}_e} \left\| \mathbf{n}^T \mathbf{C}(\mathbf{q}) \mathbf{n} \right\|. \tag{8}$$

There is a positional constraint where the end-effector of the arm should place on the physical object, defined by

$$f\left(P_x, P_z\right) = 0, \tag{9}$$

where the function, $f(x, z) = 0$ represents the profile of the physical object in x-z plane, and $\mathbf{P}_p = \left[P_x\left(\mathbf{q}_e\right), P_z\left(\mathbf{q}_e\right)\right]$ is the forward kinematic coordinate of the end-effector in x-z plane. In the following simulation carried out, the physical object is a wall defined by $f(x, z) = ax + bz + c$.

In order to obtain feasibility a few constraints are defined. To decrease the displacement of the shoulder joint α and elbow joint β and avoid singularity, the target position should be set within a range:

$$\alpha_{\min} \leq \alpha \leq \alpha_{\max} \tag{10}$$

$$\beta_{\min} \leq \beta \leq \beta_{\max}. \tag{11}$$

The ankle joint θ is underactuated and moving under the initial external force and gravitational force, thus the angle of the ankle joint, θ must be greater than the angle of the arm to ensure the arm has sufficient time to reach the target position

$$\theta_{\min} = \sin^{-1}\left(x_{CoM}/l_{CoM}\right) \tag{12}$$

$$+ \int_0^{t_f} \left[\dot{x}_{CoM}/l_{CoM} + \int_0^{t_f} g l_{CoM} \sin\theta(t) dt \right] dt, \tag{13}$$

where the x_{CoM} and $\dot{x}_{CoM}$ are the position and velocity of the CoM at the time when the fall prevention is triggered. t_f is the maximum time for the arm to reach the target position:

$$t_f = \max\left\{ \frac{\alpha_{\max}}{\omega_{\max}}, \frac{\beta_{\max}}{\omega_{\max}} \right\}, \tag{14}$$

Table 1. Model Parameters.

Parameter	Value	Description
Total mass	25 kg	
Height	0.45 m	
l_{body}	0.3762 m	from ankle joint to shoulder joint
l_{arm}	0.1782 m	sum of l_{upperarm} and l_{forearm}
l_{upperarm}	0.089 m	from shoulder joint to elbow joint
l_{forearm}	0.0892 m	from elbow joint to end-effector
K	$1e^6$ N/m	contact stiffness
B	0.6 N/(m/s)	contact damping
μ_f	0.6	contact coefficient of friction

where the maximum joint velocity $\omega_{\max}$ is constrained by the hardware. The final optimization problem is:

$$\begin{aligned} \min_{\mathbf{q}_e} \quad & \left\|\mathbf{n}^T\mathbf{C}(\mathbf{q})\mathbf{n}\right\| \\ \text{subject to} \quad & f\left(P_x, P_z\right) = 0 \\ & \mathbf{q}_{\min} \leq \mathbf{q}_{\mathrm{e}} \leq \mathbf{q}_{\max}. \end{aligned} \tag{15}$$

4 Simulation

In order to validate the proposed strategy, we test it in MATLAB & Simulink under two scenarios. The parameters of the robot are listed in Table 1. The optimal contact pose is solved by the *fmincon* function. The simulation scenarios are shown in Fig. 2 and Fig. 3 with $x_w = 0.25$ m and $x_w = 0.30$ m respectively. A horizontal impulsive force is applied to the rear of the robot, and the upper limbs' motion executes when the $\dot{x}_{CoM}$ exceeds a threshold of $\dot{x}_{th} = 0.37$ m/s.

Shown in Fig. 2 and Fig. 3, the robot is initially in a standing position with the arms naturally resting. Fig. 2(a) and Fig. 2(b) shows the robot fall forward under the external force, where the ankle angle exceeds the threshold value, thus triggering the arm motion. In Fig. 2(c) the arms have stroked the desired pose, and Fig. 2(d), finally shows the arms interaction with the wall to prevent falling. Fig. 3 replicates this, but for $x_w = 0.30$ m.

The optimized configurations are:

$$\begin{aligned} x_w = 0.25\ m: \ \mathbf{q}_{e,d1} &= [0.3000, 0.8917, 1.0014]^T \\ x_w = 0.30\ m: \ \mathbf{q}_{e,d2} &= [0.3046, 1.6652, 0.4200]^T. \end{aligned}$$

Fig. 4 shows the stiffness ellipsoid of the arms end-effector, and it can be seen that the optimized joint configuration approximately aligns the long axis of the stiffness ellipsoid with the velocity direction of the shoulder joint. Compared with Fig. 4(a), the configuration in Fig. 4(b) has a lengthier long axis stiffness ellipsoid, due to the sufficiency of space for a more stretched arm. The results correspond to our anticipated human fall arrest.

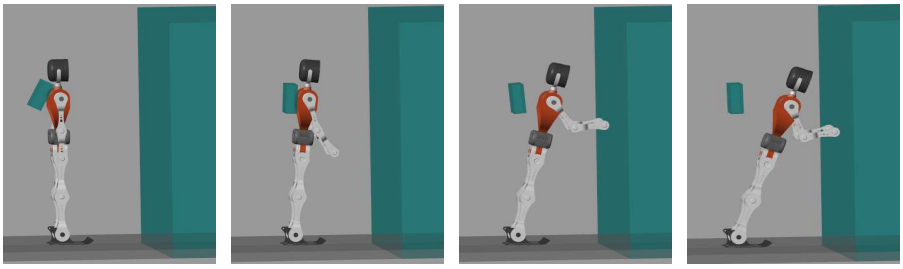

(a) 0.10 s (b) 0.20 s (c) 0.28 s (d) 0.35 s

Fig. 2. Fall prevention strategy simulation, $x_w = 0.25$ m

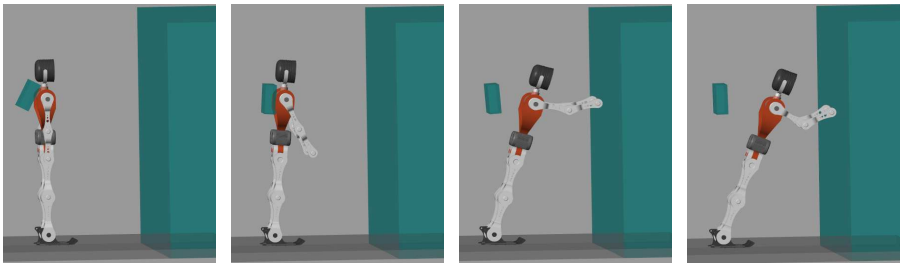

(a) 0.10 s (b) 0.20 s (c) 0.30 s (d) 0.35 s

Fig. 3. Fall prevention strategy simulation, $x_w = 0.30$ m

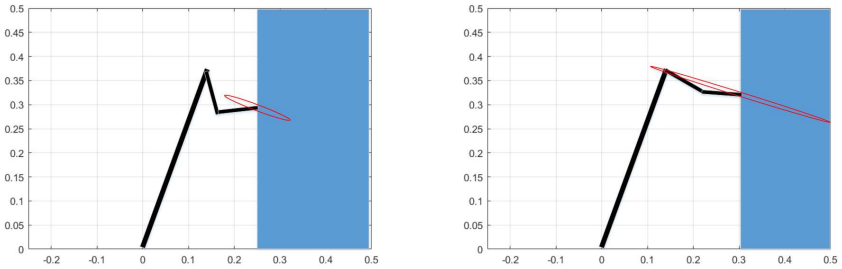

(a) $\mathbf{q}_{e,d1}$ (b) $\mathbf{q}_{e,d2}$

Fig. 4. The red line illustrate the stiffness ellipsoid of the arm

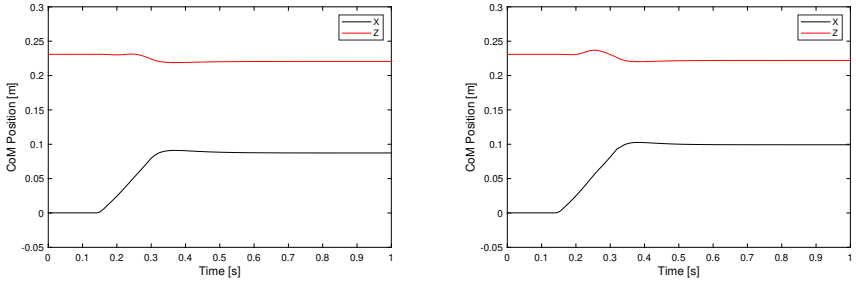

(a) $x_w = 0.25$ m (b) $x_w = 0.30$ m

Fig. 5. Position of the CoM of the robot

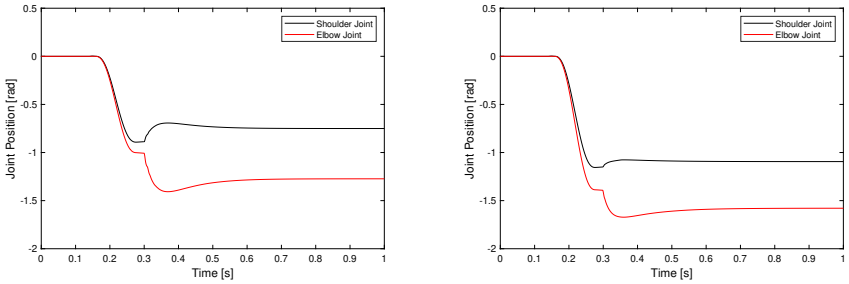

(a) with optimization (b) without optimization

Fig. 6. Variation of joint position for $x_w = 0.25$ m

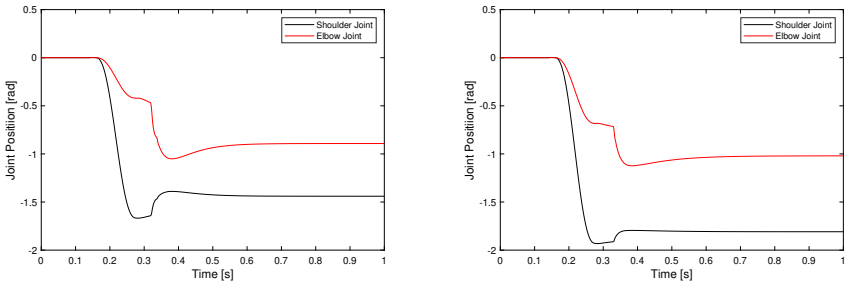

(a) with optimization (b) without optimization

Fig. 7. Variation of joint position for $x_w = 0.30$ m

In order to illustrate the detailed implementation of the strategy, we show the variation of the robot's CoM position in x-z plane with time in Fig. 5. Initially the robot stands upright, then an external is force impacted and the robot begins to fall forward. The robot falls about the axis of the ankle angle which is noticeably seen as an inverted pendulum, therefore the CoM of the robot decreases along the z-axis and moves forward along the x-axis under the effects of gravity. When the arm comes into contact with the wall, the CoM movement terminates. Fig. 6 and Fig. 7 demonstrate the variation of the shoulder joint and the elbow joint, which represents the reaction of the arm. When the fall is detected, the shoulder joint and elbow joint rotate to emulate the target position. Once contact between the arm and the wall occurs, the arm works as a damping-spring system. The arm generates a resistive force corresponding to the displacement to absorb the impact and stabilize the robot. Comparing Fig. 6(a) and Fig. 6(b), the joint without an optimized configuration changed far greater when contact occurs than with the normal configuration. This means that if there is a excessive impact, the arm may have insufficient stiffness to stabilize the robot that would result in collapse. Similar conclusions can be drawn from Fig. 7(a) and Fig. 7(b).

Fig. 8 shows the joint torque of the arm within simulation. In Fig. 8(a), the arm comes into contact with the wall with an optimized configuration, and it is seen that in order to achieve the target stiffness when contact occurs, the maximum joint torque of the shoulder and elbow joints are -12.8 Nm and 9 Nm respectively. Fig. 8(b) shows the same scenario without an optimized joint configuration. The maximum joint torques are 18.6 Nm and 13 Nm respectively, which are greater than in Fig. 8(a). Fig. 9 shows a similar result. The results demonstrate that the required joint torque is smaller with the optimized configuration for the same Cartesian stiffness of the end-effector, and also means that an optimized configuration can vary over a greater range as a limited actuator.

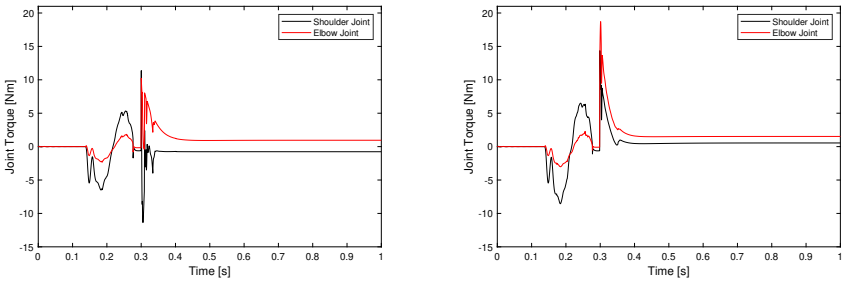

(a) with optimization (b) without optimization

Fig. 8. Variation of joint torque for $x_w = 0.25$ m

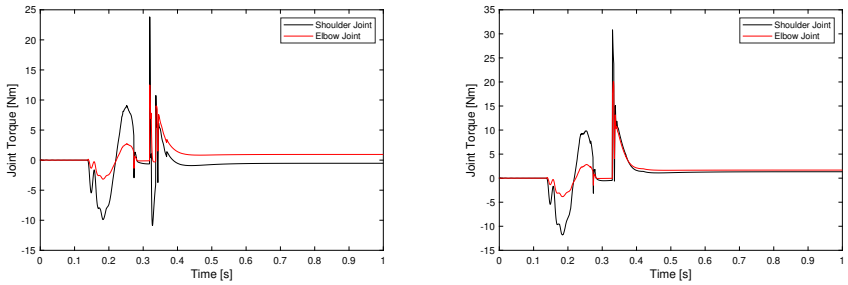

(a) with optimization (b) without optimization

Fig. 9. Variation of joint torque for $x_w = 0.30$ m

5 Conclusion

In this paper, a novel fall prevention strategy for humanoid robots using their inherent upper limbs is presented. The main concept is inspired by the fall arrest of a human; humans prefer using the direction of their respective arms stiffness ellipsoid against the direction of fall. We present an optimized algorithm used to generate arm posing, subsequently reducing the joint torque when interacting with a wall in a compliant behavioral manner. The strategy is triggered by a fall detection system, and once falling has begun, the upper limbs kinematics are generated and executed by the optimization algorithm. Finally, validation of the proposed strategy is completed via a simulation environment, and the results successfully show the strategy to be efficient and effective, where the optimal configuration shows to inherit a better performance. Future work will expand on the same strategy applied in a 3D scenario and physical tests.

Acknowledgment

This work is supported by the Engineering and Physical Sciences Research Council (Grant No. EP/R513258/1).

References

1. Ajoudani, A., Tsagarakis, N.G., Bicchi, A.: Choosing poses for force and stiffness control. IEEE Transactions on Robotics **33**(6), 1483–1490 (2017). https://doi.org/10.1109/TRO.2017.2708087
2. Borrelli, J., Creath, R., Rogers, M.W.: Protective arm movements are modulated with fall height. Journal of Biomechanics **99**, 109569 (2020). https://doi.org/10.1016/j.jbiomech.2019.109569
3. Burkhart, T.A., Andrews, D.M.: Kinematics, kinetics and muscle activation patterns of the upper extremity during simulated forward falls. Journal of Electromyography and Kinesiology **23**(3), 688–695 (2013). https://doi.org/10.1016/j.jelekin.2013.01.015

4. Butler, R.J., Crowell III, H.P., Davis, I.M.: Lower extremity stiffness: implications for performance and injury. Clinical biomechanics **18**(6), 511–517 (2003). https://doi.org/10.1016/S0268-0033(03)00071-8
5. Castano, J., Zhou, C., Tsagarakis, N.: Design a fall recovery strategy for a wheel-legged quadruped robot using stability feature space. In: IEEE International Conference on Robotics and Biomimetics. pp. pp. 41–46 (2019). https://doi.org/0000-0002-6677-0855
6. Chiu, J., Robinovitch, S.N.: Prediction of upper extremity impact forces during falls on the outstretched hand. Journal of Biomechanics **31**(12), 1169–1176 (1998). https://doi.org/10.1016/S0021-9290(98)00137-7
7. Chou, P.H., Chou, Y.L., Lin, C.J., Su, F.C., Lou, S.Z., Lin, C.F., Huang, G.F.: Effect of elbow flexion on upper extremity impact forces during a fall. Clinical Biomechanics **16**(10), 888–894 (2001). https://doi.org/10.1016/S0268-0033(01)00086-9
8. DeGoede, K., Ashton-Miller, J., Schultz, A.: Fall-related upper body injuries in the older adult: a review of the biomechanical issues. Journal of Biomechanics **36**(7), 1043–1053 (2003). https://doi.org/10.1016/S0021-9290(03)00034-4
9. Hoffman, E.M., Perrin, N., Tsagarakis, N.G., Caldwell, D.G.: Upper limb compliant strategy exploiting external physical constraints for humanoid fall avoidance. In: IEEE-RAS International Conference on Humanoid Robots. pp. 397–402 (2013). https://doi.org/10.1109/HUMANOIDS.2013.7030005
10. Hsu, H.H., Chou, Y.L., Lou, S.Z., Huang, M.J., Chou, P.P.H.: Effect of forearm axially rotated posture on shoulder load and shoulder abduction/flexion angles in one-armed arrest of forward falls. Clinical Biomechanics **26**(3), 245–249 (2011). https://doi.org/10.1016/j.clinbiomech.2010.10.006
11. Kim, K.J., Ashton-Miller, J.A.: Biomechanics of fall arrest using the upper extremity: age differences. Clinical Biomechanics **18**(4), 311–318 (2003). https://doi.org/10.1016/S0268-0033(03)00005-6
12. Latash, M.L., Zatsiorsky, V.M.: Joint stiffness: Myth or reality? Human Movement Science **12**(6), 653–692 (1993). https://doi.org/10.1016/0167-9457(93)90010-M
13. Lattimer, L., Lanovaz, J., Farthing, J., Madill, S., Kim, S., Robinovitch, S., Arnold, C.: Biomechanical and physiological age differences in a simulated forward fall on outstretched hands in women. Clinical biomechanics **52**, 102–108 (2018). https://doi.org/10.1016/j.clinbiomech.2018.01.018
14. Li, Z., Zhou, C., Zhu, Q., Xiong, R.: Humanoid balancing behavior featured by underactuated foot motion. IEEE Transactions on Robotics **33**(2), 298–312 (2017). https://doi.org/10.1109/TRO.2016.2629489
15. Pratt, J., Carff, J., Drakunov, S., Goswami, A.: Capture point: A step toward humanoid push recovery. In: IEEE-RAS International Conference on Humanoid Robots. pp. 200–207 (2006). https://doi.org/10.1109/ICHR.2006.321385
16. Samy, V., Caron, S., Bouyarmane, K., Kheddar, A.: Post-impact adaptive compliance for humanoid falls using predictive control of a reduced model. In: IEEE-RAS International Conference on Humanoid Robots. pp. 655–660 (2017). https://doi.org/10.1109/HUMANOIDS.2017.8246942
17. Samy, V., Kheddar, A.: Falls control using posture reshaping and active compliance. In: IEEE-RAS International Conference on Humanoid Robots. pp. 908–913 (2015). https://doi.org/10.1109/HUMANOIDS.2015.7363469
18. Wang, J., Whitman, E.C., Stilman, M.: Whole-body trajectory optimization for humanoid falling. In: American Control Conference. pp. 4837–4842 (2012). https://doi.org/10.1109/ACC.2012.6315177

19. Wang, R., Hudson, S., Li, Y., Wu, H., Zhou, C.: Normalized neural network for energy efficient bipedal walking using nonlinear inverted pendulum model. In: IEEE International Conference on Robotics and Biomimetics. pp. 1399–1405 (2019). https://doi.org/10.1109/ROBIO49542.2019.8961646
20. Wang, S., Hauser, K.: Real-time stabilization of a falling humanoid robot using hand contact: An optimal control approach. In: IEEE-RAS International Conference on Humanoid Robots. pp. 454–460 (2017). https://doi.org/10.1109/HUMANOIDS.2017.8246912
21. Yi, S.J., Zhang, B.T., Hong, D., Lee, D.D.: Online learning of low dimensional strategies for high-level push recovery in bipedal humanoid robots. In: IEEE International Conference on Robotics and Automation. pp. 1649–1655 (2013). https://doi.org/10.1109/ICRA.2013.6630791
22. Yun, S.k., Goswami, A.: Tripod fall: Concept and experiments of a novel approach to humanoid robot fall damage reduction. In: IEEE International Conference on Robotics and Automation. pp. 2799–2805 (2014). https://doi.org/10.1109/ICRA.2014.6907260
23. Zhou, C., Li, Z., Castano, J., Dallali, H., Tsagarakis, N., Caldwell, D.: A Passivity Based Compliance Stabilizer for Humanoid Robots. In: IEEE International Conference on Robotics and Automation. pp. 1487–1492 (2014). https://doi.org/10.1109/ICRA.2014.6907048